chemistry

MDPI

Article

High Thermal Stability of Enzyme-MOF Composites at 180 °C

Shitong Cui [1] and Jun Ge [1,2,*]

[1] Key Lab for Industrial Biocatalysis, Ministry of Education, Department of Chemical Engineering, Tsinghua University, Beijing 100084, China; cuishitong1998@163.com
[2] Institute of Biopharmaceutical and Health Engineering, Tsinghua Shenzhen International Graduate School, Shenzhen 518055, China
* Correspondence: junge@mail.tsinghua.edu.cn

Abstract: Encapsulating enzymes in a tailored scaffold is of great potential in industrial enzymatic catalysis, which can enhance the stability of enzymes thus expanding their applications. Metal–organic frameworks (MOFs) are emerging as promising candidates for enzyme encapsulation due to their precise pore structure, ease of synthesis and good biocompatibility. Despite the fact that enzymes encapsulated in MOFs can obtain enhanced stability, there has been little discussion about the thermal stability of enzyme-MOF composites in solid state under extremely high temperatures. Herein, we fabricated the enzyme-MOF composites, CALB-ZIF-8, via a convenient coprecipitation method in aqueous solution, which exhibited good thermal stability at 180 °C. It was found that the activity of CALB encapsulated in ZIF-8 retained nearly ~80% after heating for 10 min at 180 °C. A finite element method was applied to investigate the heat transfer process within a ZIF-8 model, indicating that the air filled in cavities of ZIF-8 played a significant role in hindering the heat transfer and this may be an important reason for the outstanding thermal stability of CALB-ZIF-8 at 180 °C, which paves a new path for expanding the industrial application of enzyme-MOF composites.

Keywords: metal–organic frameworks; encapsulated enzymes; thermal stability; finite element analysis

Citation: Cui, S.; Ge, J. High Thermal Stability of Enzyme-MOF Composites at 180 °C. *Chemistry* **2023**, *5*, 2025–2037. https://doi.org/10.3390/chemistry5030137

Academic Editors: Di Li, Michael EG Lyons and Valentina Gargiulo

Received: 29 June 2023
Revised: 12 September 2023
Accepted: 17 September 2023
Published: 19 September 2023

1. Introduction

As an essential catalyst in bioprocesses, enzymes can accelerate a wide range of biological conversions in a green and efficient manner and nowadays are also increasingly applied in industrial processes to produce fine chemicals, drugs and materials [1]. Therefore, biomanufacturing has been considered a powerful complement to traditional chemical synthesis [2]. However, the fact remains that the stable three-dimensional structure of enzymes will be easily disrupted under harsh conditions such as high temperatures, organic solvents and extreme pH, resulting in a severe deactivation of enzymes, which hinders their industrial applications. How to improve the stability of enzymes during use is a significant and persistent issue in enzyme research [3].

A promising solution to this issue is to design a tailored scaffold to protect enzyme structure, including polymers [4], DNA [5], nano-flowers [6], metal–organic frameworks (MOFs) [7] and others. It has been proved that the confined microenvironment provided by the scaffold can help to stabilize the enzyme structure, thus improving its stability [8]. Among them, MOFs are emerging as promising candidates due to their high surface area, good structural rigidity and fine biocompatibility [9–11]. In 2014, the Ge group [12] first proposed a one-pot coprecipitation method to fabricate enzyme-MOF composites in methanol solution where cytochrome c (Cyt c) was encapsulated in zeolitic imidazolate framework-8 (ZIF-8) after the polyvinylpyrrolidone (PVP) modification to improve the dispersion and stabilization of Cyt c in methanol. It was found that both the activity and stability of Cyt c were enhanced after encapsulation in ZIF-8, which was attributed to the conformational change induced by methanol incubation and confinement in MOFs. In addition, it is worth mentioning that the encapsulation of enzymes in MOFs can also be conducted in aqueous

solution. Falcaro and coworkers [13,14] proposed that biomacromolecules could facilitate the formation of MOFs under physiological conditions via a biomimetic mineralization process, where biomacromolecules such as enzymes would have a high affinity for the precursors of MOFs in aqueous solution, thus inducing the slow growth of MOF crystals around them to form the final hybrid structure. Therefore, the structure rigidity and confinement effect of MOFs can significantly improve the stability of embedded enzymes. It was proved that urease and horseradish peroxidase (HRP) embedded in MOFs could effectively retain their activity after being treated at 80 °C and boiled in dimethylformamide, respectively [14].

Recently, more versatile and general strategies for encapsulating enzymes in MOFs have been deeply studied, including coordination defects [15], modification of surface charge [16,17], microfluidic synthesis [18,19], competitive coordination [20] and others. In addition, various structures such as amorphous and defective MOFs have been fabricated and applied in biosensing [17], biocatalysis [21] and drug delivery [15].

However, with the expanding applications of enzymatic catalysis, the requirements for enzyme stability are continuously increasing. For example, Xu and coworkers [22,23] provided an innovative demonstration that nanoscopically dispersing enzymes in polyesters would trigger the chain-end-mediated depolymerization thus speeding up the degradation of polyester plastics in natural environments. This interesting discovery was promising to open up new opportunities to solve the white pollution. Nevertheless, a significant factor hindering its application is the poor thermal stability of enzymes because plastics are usually processed and moulded under extremely high temperatures which are usually above their melting points, whereas free enzymes usually tend to lose their activity under these harsh conditions, thus leading to a decreased effect on the degradation of polyester plastics. For example, Iwata and coworkers [24] demonstrated that directly adding Proteinase K (ProK), an enzyme which has the activity to hydrolyze poly lactic acid (PLA), in the extruded PLA film under 200 °C would not accelerate the degradation due to the deactivation of enzymes.

Therefore, this existing problem encouraged us to investigate the thermal stability of enzyme-MOF composites in dry conditions at 180 °C, which has already exceeded the melting point of most polyester plastics. To the best of our knowledge, although enzymes encapsulated in MOFs have been proven to possess higher stability when dispersed in aqueous solution, there has been little discussion focusing on the thermal stability of enzyme-MOF composites in dry conditions under such a high temperature. Herein, we synthesized enzymes encapsulated ZIF-8 taking Candida antartica lipase B (CALB, a lipase which has the activity to hydrolyze polyester plastics [22,23]) as an example (noted as CALB-ZIF-8) via a one-pot coprecipitation process and then developed a method to investigate their thermal stability in dry conditions at 180 °C. Furthermore, a finite element model was developed to simulate the heat transfer process within the enzyme-MOF composites, as an approach to better understand the experiments. This study is promising in expanding a wider application and long-term catalysis of enzyme-MOF composites in industrial processes with extremely high temperatures.

2. Materials and Methods

2.1. Materials

Zinc acetate dihydrate (≥99.0) and 4-nitrophenyl butyrate (p-NPB) were purchased from Sigma-Aldrich (Shanghai, China). 2-Methylimidazole (2-MeIm, 99%) was purchased from Acros Organics (Shanghai, China). Phosphate buffer (PB), Tris-HCl buffer and ethylene diamine tetraacetic acid (EDTA) solution were purchased from Solarbio (Beijing, China). Acetone was purchased from Beijing Tongguang fine chemicals company (Beijing, China). Bradford protein assay kit was purchased from Solarbio (Beijing, China). CALB was purchased from Nanjing Ranxi Biotechnology Co., Ltd (Nanjing, China). CALB was purified through dialysis using a 10 kDa cutoff semi-permeable membrane before use. Other reagents were used without further purification.

2.2. Synthesis of CALB-ZIF-8

CALB-ZIF-8 were synthesized according to the one-pot coprecipitation method developed by our group previously [12,25] with slight modification. A schematic showing this coprecipitation process is shown in Figure 1. In detail, 200 μL of CALB solution (20 mg CALB powder/mL) and 200 μL of $Zn(OAc)_2$ solution (0.8 M) were simultaneously added into 2 mL of 2-MeIm solution (1.6 M) and then stirred (500 rpm) at room temperature for 30 min. The precipitate was collected by centrifugation at 12,000 rpm for 5 min and then washed at least three times with deionized water to remove unreacted molecules. The supernatant and washing solutions were stored for the next protein assays (i.e., measurement of enzyme amount and activity). CALB-ZIF-8 powders were finally obtained by lyophilization overnight. ZIF-8 was synthesized following the same procedure as above without the addition of enzymes.

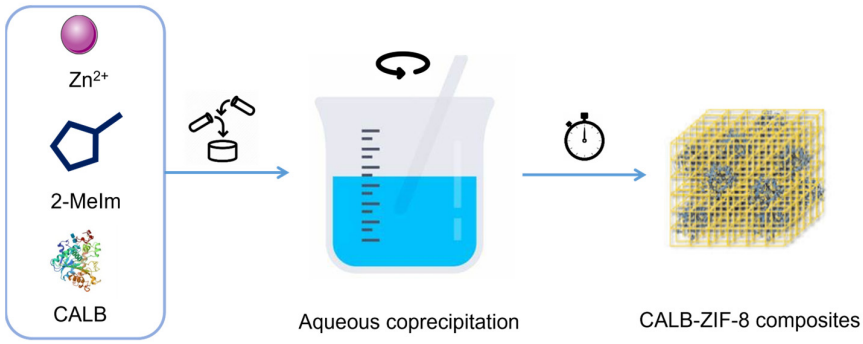

Figure 1. Schematic showing the synthesis of CALB-ZIF-8 composites.

2.3. Characterizations

Micromorphology of CALB-ZIF-8 was observed by scanning electron microscopy (SEM) and transmission electron microscopy (TEM) analysis. For SEM analysis, samples were coated on the conducting resin and then observed on a JSM401 SEM with an accelerating voltage of 5 kV. For TEM analysis, samples were fully suspended in ethanol and a drop of the suspension was added onto a carbon grid and then dried at room temperature overnight for testing. TEM images were taken by a JEOL JEM-2010 high-resolution TEM with an accelerating voltage of 120 kV. Powder X-ray Diffraction (XRD) patterns were recorded using a Bruker D8 Advance X-ray diffractometer with a Cu Kα anode (λ = 0.15406 nm) at 40 kV and 40 mA. The scanning speed was 5°/min and the diffraction angle ranged from 5 to 45°. Thermal gravimetric analysis (TGA) was performed on a TA Instruments TGA 2050 thermogravimetric analyzer where samples were heated at a constant temperature of 180 °C for 10 min in an air atmosphere. Circular dichroism (CD) spectroscopy was performed on Chirascan Plus (version 1.0) where the CD signal from 190 to 260 nm was collected to compare the secondary structure of free CALB and released CALB after heating with the crude CALB (unheated).

2.4. Determination of Enzyme Immobilization Yield

The enzyme immobilization yield was defined as the ratio of the encapsulated amount of enzyme in ZIF-8 to the total amount of enzyme employed, which could be calculated using the following equation:

$$Y = \frac{T - S}{T} \times 100\% \quad (1)$$

where Y is the immobilization yield, T is the total amount of enzyme employed in the initial solution, and S is the amount of enzyme in the supernatant and washing solutions. The amount of enzyme was quantified using the Bradford protein assay kit with bovine serum albumin (BSA) as standard.

2.5. Release of CALB from CALB-ZIF-8

CALB-ZIF-8 (5 mg) was dispersed in 2 mL phosphate buffer (PB, 50 mM, pH = 6) and the system was stirred for 6 h at room temperature, for a pH-triggered release of CALB. The supernatant was collected by centrifugation at 12,000 rpm for 5 min. The enzyme amount and activity of CALB released in the supernatant after dissolving the ZIF-8 skeleton were then measured to determine the release percentage and activity recovery. The enzyme release percentage was defined as the ratio of the enzyme amount in the supernatant to the total amount of enzyme employed in the test, while the activity release percentage was defined as the ratio of activity in the supernatant to the total activity employed. It was worth noting that the pH-triggered release is a dynamic equilibrium process due to the fact that 2-methylimidazole produced by the dissolution of ZIF-8 would increase the pH thus inhibiting the release process [25,26].

2.6. Measurement of Enzyme Activity

The activity of CALB (including the free CALB as well as CALB released from ZIF-8 in solution) was measured using p-NPB as substrates. In detail, 2 μL of p-NPB was first dissolved in 1 mL acetone and then diluted with 20 mL phosphate buffer (PB, 50 mM, pH 7.0) to obtain the substrate solution. In a typical testing, 50 μL of enzyme solution was added to 950 μL of substrate solution to initiate the reaction and the system was vortexed for ~5 s to ensure an adequate mass transfer. Then the mixture was immediately transferred into a 1 mL quartz cuvette and the absorbance at 348 nm [12,15] for 15 s was recorded using UV−vis spectroscopy. One unit of CALB activity was defined as the amount of CALB which could hydrolyze 1 μmol of p-NPB per minute under the assay conditions. The same protocol was applied to determine the enzymatic activity of immobilized CALB where the CALB-ZIF-8 solution was firstly sonicated for ~30 s to ensure a uniform dispersion before being mixed with the substrate solution. The relative activity of CALB-ZIF-8 was calculated based on the same protein concentration where the activity of crude CALB was regarded as 100%. The protein amount was quantified using the Bradford protein assay kit before measuring the activity.

2.7. Measurement of Thermal Stability

The thermal stability of free CALB and CALB-ZIF-8 powders under extremely high temperatures was measured using a laboratory hot press. Typically, the temperature of heating plates was set as 180 °C. Then samples covered with aluminium foil were placed on the plate and heated for different times. All samples were dried at vacuum to a constant weight at 37 °C before heat treatment. The enzyme activity of free CALB and released CALB from ZIF-8 after heating was also measured following the same protocol as described in Sections 2.5 and 2.6 where the activity of CALB-ZIF-8 after heating was not measured in order to exclude the mass transfer resistance brought by ZIF-8. It was worth noting that the samples were immediately mixed with the buffer for activity testing after being taken out from the hot press. The relative activity was calculated based on the same protein concentration where the activity of samples before heating was regarded as 100%.

2.8. Simulation Models

The simulation model of ZIF-8 was developed based on the following assumptions:

✓ A ZIF-8 particle was composed of a number of repeating and regular representative volume elements (RVEs), the thermal conductivity of which is equal to the thermal conductivity of the material as a whole;
✓ ZIF-8 particles were tightly connected to each other by connections of RVEs, ignoring the air between ZIF-8 particles;
✓ Only heat transfer processes were considered in this model, ignoring the heat radiation and heat convection;
✓ The pore size and porosity of ZIF-8 were valued as 2 nm and 80%, respectively, according to the previous report [15,27];

✓ A single RVE cell in this model was modeled as a 100 nm × 100 nm × 100 nm cube, which was close to a single ZIF-8 particle under SEM.

2.9. Simulation of Heat Transfer Process

The heat transfer process within the model was simulated using COMSOL Multiphysics. The boundary conditions were set as follows: the right end section of the model was set as the thermostatic boundary with the temperature inlet T = 180 °C (high-temperature side) while the left end section of the model was set as the thermostatic boundary with the temperature outlet T = 25 °C (low-temperature side).

Additionally, two different situations based on the ZIF-8 model were specifically investigated and compared:

✓ Situation 1: air filling assumption, where cavities of the model were filled with air (which corresponded to the actual situation);
✓ Situation 2: no air filling assumption, where cavities of the model were filled with the same material as the wall;

Transient thermal analysis was performed for these two situations until the heat transfer within the model reached the steady state (where the temperature at various locations within the model did not vary with time).

3. Results and Discussion

3.1. Synthesis and Characterization of CALB-ZIF-8

CALB-ZIF-8 were synthesized via the previously reported one-pot coprecipitation method [12,25] in an aqueous solution to form a crystalline framework around enzymes, as shown in Figure 1.

To evaluate the immobilization efficiency of this process, enzyme amount before and after immobilization was quantified by Bradford protein assay kit, which was shown in Table 1. The amount of immobilized enzyme could be obtained by the difference between the total amount of enzyme employed and the amount of enzyme in supernatant and washing solutions. When measuring the enzyme amount, each sample was tested 3 times and the average immobilization yield was calculated to be 66.2% (the calculation of immobilization yield can be seen in Section 2.4).

Table 1. Evaluation of the immobilization yield of CALB-ZIF-8.

Code	Total Enzyme Employed (mg) [1]	Enzyme in Supernatant (mg) [2]	Averaged Immobilization Yield (%)
CALB-ZIF-8	1.004 ± 0.009	0.335 ± 0.015	66.2 ± 0.9

[1] Enzyme amount was quantified by Bradford protein assay kit. [2] Washing solutions contained.

Morphologies of the as-synthesized CALB-ZIF-8 are shown in Figure 2. Scanning electron microscopy (SEM) images showed that CALB-ZIF-8 were uniformly distributed with an average size of ~100 nm (Figure 2a), which exhibited a standard rhombic dodecahedral morphology as ZIF-8 [28], indicating that the addition of CALB would not affect the crystal structure of ZIF-8. Transmission electron microscopy (TEM) images (Figure 2b) also demonstrated the polygonal crystal structure of CALB-ZIF-8, which agreed well with SEM images. Energy-dispersive spectrum (EDS) mapping (Figure S1) demonstrated a uniformly distributed signal of Zn and S from ZIF-8 and CALB, respectively, further confirming that CALB was successfully encapsulated in ZIF-8.

XRD patterns of the as-synthesized CALB-ZIF-8 were shown in Figure S2 where the well-preserved crystallinity of ZIF-8 was observed, indicating that encapsulated CALB did not change the crystal structure of the scaffold.

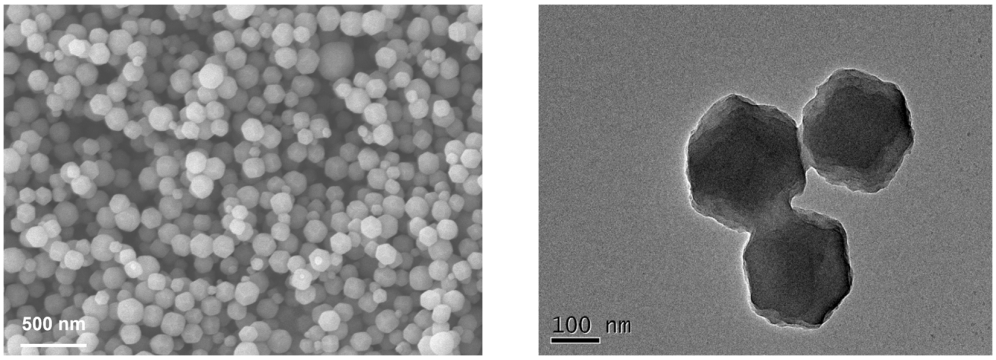

(**a**) (**b**)

Figure 2. Morphology characterization of CALB-ZIF-8: (**a**) SEM images; (**b**) TEM images.

To evaluate the enzymatic activity of CALB-ZIF-8, we chose 4-nitrophenyl butyrate (p-NPB) as substrate, which can be hydrolyzed by CALB and the hydrolysis product (p-nitrophenol) has a characteristic absorption peak at 348 nm. By monitoring the rate of product generation (slope of the kinetic curve), the activity of enzymes can be calculated (shown in Table 2).

Table 2. Evaluation of the enzyme activity of CALB-ZIF-8.

Code	Total Activity Immobilized (U) [1]	Apparent Activity (U) [2]	After 6 h Release in PB Buffer	
			Enzyme Release (%)	Activity Release (%)
CALB-ZIF-8	3640 ± 168	434 ± 21	38.2 ± 0.3	34.6 ± 1.7

[1] Calculated by the difference between the total enzyme activity employed and the activity in the supernatant and washing solutions. [2] Activity of CALB-ZIF-8 measured according to the method in Section 2.6 ("apparent" referred to taking the internal diffusion resistance provided by ZIF-8 skeleton into consideration).

Herein, one unit of CALB activity was defined as the amount of CALB which could hydrolyze 1 μmol of p-NPB per minute under the assay conditions, where the activity of free CALB was evaluated as ~5330 U/mg according to this method. Therefore, by measuring the amount and activity of an enzyme in the supernatant and washing solutions, the total activity immobilized in ZIF-8 was calculated to be ~3640 U and the activity immobilization yield was ~68.3% where the activity immobilization yield was defined as the ratio of the enzyme activity encapsulated in ZIF-8 to the total activity employed, which was close to the enzyme immobilization yield.

As shown in Table 2, although there was a high activity immobilization yield of ~68.3%, the as-synthesized CALB-ZIF-8 exhibited an apparent activity of only ~434 U and a relative activity of 11.9% (defined as the ratio of apparent activity to the total activity immobilized), which was because that the microporous structure of ZIF-8 seriously hindered the substrate transportation thus reducing the apparent activity (indicating an internal diffusion resistance existed in CALB-ZIF-8), and this phenomenon was also observed in previous research about CALB-ZIF-8 [15,29].

An advantageous property of ZIF-8 is its good stimulus–response performance and it is known that the crystal structure of ZIF-8 can be dissolved in phosphate-buffered saline (PBS) media [26] or in the presence of ethylene diamine tetraacetic acid (EDTA) [30] or in other moderate acidic conditions (such as pH range 5–6) [31,32], thus leading to the release of encapsulated enzymes, which can be used for the smart cargo release.

Therefore, we checked the response release property of CALB-ZIF-8 by immersing CALB-ZIF-8 in PB buffer (pH = 6) for 6 h. The release percentage of enzyme amount/activity was calculated as the ratio of enzyme amount/activity in the supernatant to the total amount/activity of enzyme employed in the test (shown in Table 2). It was illustrated in Table 2 that there was an approximately 38.2% enzyme release and 34.6% activity

release from CALB-ZIF-8, respectively, after a 6 h emersion in PB buffer, indicating a good response release property of CALB-ZIF-8. In addition, the activity of CALB released to the supernatant was evaluated as ~4828 U/mg, which was nearly ~90% of the original. This result indicated that the encapsulation process in ZIF-8 hardly affected the activity of CALB itself, despite a decrease in apparent activity.

3.2. Thermal Stability of CALB-ZIF-8 under Extremely High Temperature

Previous studies [14] have proved that enzyme-ZIF-8 composites can maintain their activity better than free enzymes under high temperatures or in the existence of organic solvents. However, these experiments were usually conducted in aqueous solution, which means that the temperature would not exceed the boiling point of water (usually <100 °C). Therefore, it still remains unknown whether enzyme-ZIF-8 composites will retain their activity under higher temperatures (>100 °C) in dry conditions, which may contribute to a broader industrial application of enzymatic catalysis.

Therefore, as a proof of concept, we investigated the thermal stability of CALB-ZIF-8 in dry conditions under 180 °C, which has exceeded the melting point of most biodegradable plastics. To the best of our knowledge, the highest temperature in the literature was reported by Falcaro and coworkers [14], where the immobilized biocatalyst was treated in boiling dimethylformamide (DMF) at a temperature of 153 °C. However, differing from what has been reported in the literature, the focus of our study is on the thermal stability of enzyme-MOF composites in the solid state to mimic the plastic extrusion process, and that is why we chose 180 °C as the assay temperature.

As shown in Figure 3, the experiment was conducted on a laboratory hot press (Figure 3a) where samples were placed on a metal heating plate after being covered with aluminum foil to avoid heat radiation and heat convection. Therefore, heat was only transferred from the heating plate to samples by heat conduction.

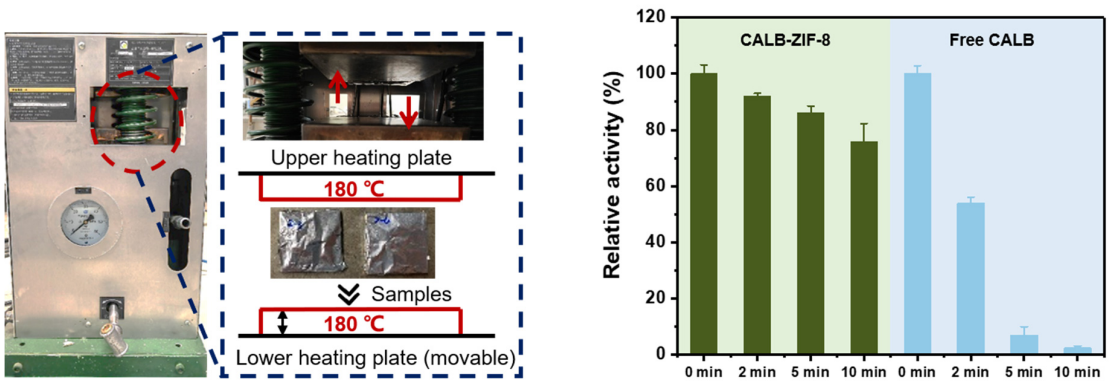

(**a**) (**b**)

Figure 3. Thermal stability of CALB-ZIF-8 composites: (**a**) laboratory hot press to conduct the experiment (where arrows inside the figure indicate the upper and lower heating plates); (**b**) relative activity of CALB-ZIF-8 and free CALB after heating for different times under 180 °C, where in this place CALB-ZIF-8 refers to the released CALB from ZIF-8 skeleton in the supernatant, in order to obtain an intuitive comparison with free CALB.

It was shown in Figure 3b that the relative activity of CALB-ZIF-8 could retain nearly ~80% after heating at 180 °C for 10 min while free CALB was almost inactive under the same condition, indicating the outstanding thermal stability of CALB-ZIF-8 under extremely high temperature, where the activity of embedded CALB could be well-maintained. Herein, the activity of CALB-ZIF-8 referred to the activity of CALB released from ZIF-8, in order to exclude the internal mass transfer resistance of the ZIF-8 skeleton and thus obtain a more intuitive comparison with the activity of free CALB. Actually, it was worth mentioning

that a longer time to perform the assay would provide better proof for the gain in thermal stability. However, as mentioned in the introduction part, what encouraged us to investigate the stability of enzyme-MOF composites at 180 °C was the poor thermal stability of free enzymes during the plastic extrusion process. Typically, this extrusion process will not take such a long time, usually 2–5 min, to avoid the thermal aging of plastics and this residence time in the extruder is also enough for the melt blending, so that is why we chose 10 min as the maximum assay time.

This outstanding thermal stability may arise from the rigidity of the ZIF-8 scaffold. Through the SEM images (Figure S3) and XRD patterns (Figure S4), it was found that the micromorphology and crystal structure of CALB-ZIF-8 remained unchanged after heating at 180 °C thus protecting enzymes from being destroyed by high temperature.

From the macroscopic view, it was demonstrated that free CALB powders underwent obvious surface carbonization upon high-temperature heating, yet the appearance of CALB-ZIF-8 did not change significantly (Figure S5), which corresponds to the result in Figure 3b.

In addition, from the microscopic view, we also tried to investigate the possible mechanism of the higher thermal stability of CALB-ZIF-8 at 180 °C. Actually, the content of hydration water within enzymes is essential for their activity performance. Therefore, to evaluate the change of hydration water during the heating process, TGA was performed to continuously record the mass change of samples when heated at 180 °C for 10 min, which was consistent with the testing conditions of thermal stability. As shown in Figure S6, it was found that there was no significant difference in the mass change between CALB (98.76 wt% mass residue) and CALB-ZIF-8 (99.44 wt% mass residue) after being heated at 180 °C for 10 min, indicating that there was almost no difference in the content of water between CALB and CALB-ZIF-8 under this condition. Furthermore, the conformational change of protein has also been considered as another key factor affecting their activity, so CD spectroscopy was also performed to compare the secondary structure of free CALB and CALB released from CALB-ZIF-8 after heating at 180 °C for 10 min with that of the crude CALB (unheated). The CD results shown in Figure S7 illustrated that the encapsulation of CALB in ZIF-8 would well protect their secondary structure from being significantly changed when heated at 180 °C for 10 min while free CALB underwent an obvious structural change at the same condition, indicating that the rigidity structure of ZIF-8 may be helpful for the maintenance of enzyme structure under high temperature, which may be corresponding to the higher thermal stability of CALB-ZIF-8 at 180 °C.

3.3. Finite Element Simulation of Heat Transfer within ZIF-8

This outstanding thermal stability of CALB-ZIF-8 at 180 °C encouraged us to further investigate the heat transfer process within the composites. The finite element method (FEM), which has been widely applied in the simulation of macro chemical processes, is a numerical method to solve thermal, force or electromagnetic issues by considering a continuum as a discretized collection of several finite-sized unitary bodies. Herein, FEM was utilized to simulate the heat transfer process within ZIF-8.

The first step to conducting FEM simulation is to construct a finite element model of ZIF-8. It is known that ZIF-8 is a porous material where the framework is connected by zinc ions and imidazole ligands and the cavity is filled with air. Therefore, ZIF-8 possess a high surface area and porosity, which gives them excellent performance in the field of gas adsorption and separation [33]. Herein, we abstracted the ZIF-8 structure as a scaffold-like model based on the schematic shown in Figure 4 and assumed that a single representative volume element (RVE) cell was a 100 nm × 100 nm × 100 nm cube (in the middle of Figure 4), which was close to the average size of a single ZIF-8 particle in Figure 2a. It was not difficult to understand that the simulation of this 3D model could be regarded as a stretching of the 2D cross-section (in the right of Figure 4), with the assumption that heat was only transferred in one direction.

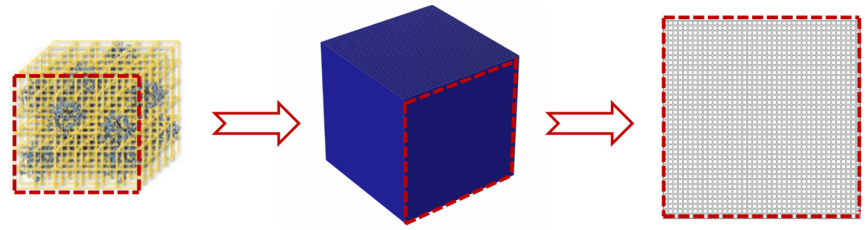

Figure 4. Development of simulation model for ZIF-8.

In the 2D cross-section model shown in Figure 4, the wall and cavities represented the skeleton and pores of ZIF-8, respectively. According to the assumptions in Section 2.8, the wall thickness was valued as 0.5 nm and the cavity width was valued as 2 nm, where we assumed that the average pore size of ZIF-8 was 2 nm and the porosity was 80%.

The boundary conditions were set as follows. The right-end cross-section of the model was set as the thermostatic boundary with the temperature inlet T = 180 °C (high-temperature side) and the left-end cross-section was set as the thermostatic boundary with the temperature outlet T = 25 °C (low-temperature side). These conditions were set with the aim of simulating the state of samples heating in a hot press.

The physical properties of ZIF-8 were determined by the combination of experimental measurements and the literature reports [34,35], which are shown in Table 3.

Table 3. Physical properties of ZIF-8.

Properties	Unit	Value
Thermal conductivity	$W \cdot m^{-1} \cdot K^{-1}$	0.165
Density [1]	$g \cdot cm^{-3}$	1.87
Specific heat capacity [2]	$J \cdot g^{-1} \cdot C^{-1}$	2.20

[1] True density was measured by gas displacement method. [2] Specific heat capacity was measured by DSC sapphire method.

Specifically, the transient thermal analysis was applied during the simulation, in which the temperature at any point would change and converge to a constant value over time when calculations reached a steady state. The temperature distribution within the model under the steady state is shown in Figure 5. It was illustrated in Figure 5 that the temperature decreased uniformly from 180 °C (the right end) to 25 °C (the left end) which was attributed to the constant temperature difference between these two sections. Therefore, the temperature would show a gradient distribution within the model when calculations converged.

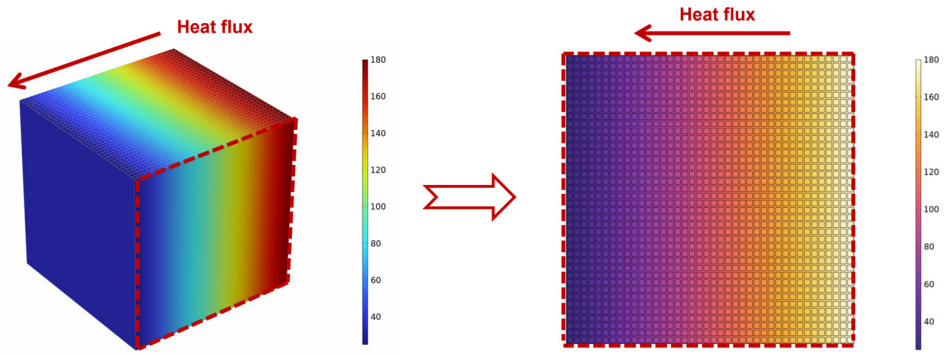

Figure 5. Temperature distribution within the model when calculations reached the steady state.

To further investigate the heat transfer process within ZIF-8, two more situations were considered and compared based on this model, which were the air-filling situation and no air-filling situation, respectively (see Section 2.9). In addition, it is worth noting that the

thermal conductivity of air is about 0.02~0.03 $W \cdot m^{-1} \cdot K^{-1}$, which is far less than that of ZIF-8. Therefore, the air-filled cavities could be considered as an adiabatic state.

Temperatures of cross-sections at different locations during the simulation process were recorded which was shown in Figure 6. By comparing these two situations, it could be found that the situation with air filling inside the cavities (air-filling assumption, dashed line in the figure) took a longer time to reach the steady state, which was due to the barrier effect of air on heat, making the heat transfer rate slower. Therefore, the temperature in the air-filling situation would be lower than that in the no air-filling situation at the same cross-section and at the same moment before reaching the steady state. However, when the simulation converged, the temperatures at the same cross-section were identical for both situations, which was because the same boundary conditions were applied and there was no internal heat source in this model, and this result further confirmed the reliability of the simulation.

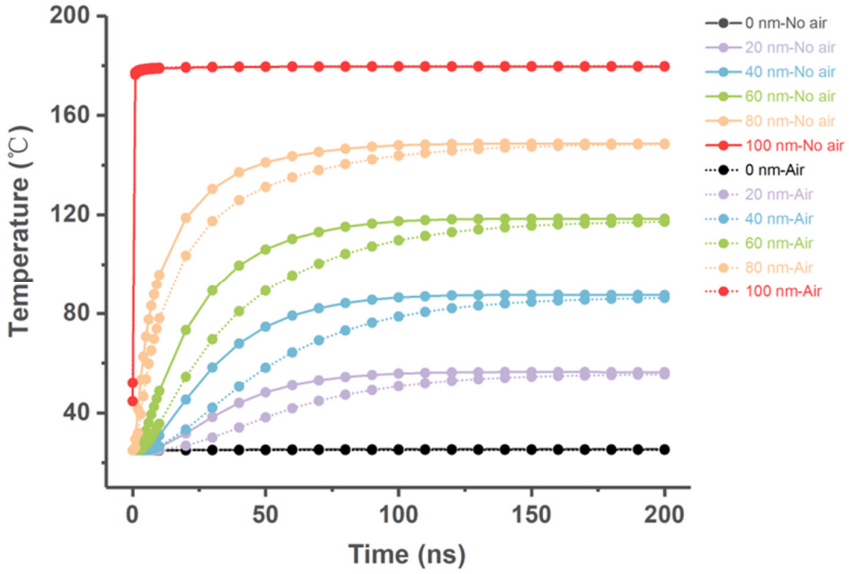

Figure 6. Temperatures at different locations during the simulation as a function of time in two different situations.

The simulation results indicated that the air filled in ZIF-8 cavities exhibited a significant effect on hindering the heat transfer. Therefore, the heat flux, which refers to the rate of heat transferring through per unit area, of these two situations after reaching the steady state was calculated. As shown in Figure 7, when there was air filling in cavities of the ZIF-8 model, the heat flux was nearly 1/5 of that without air filling, which was another proof of the heat-hindering effect of the air in ZIF-8.

Based on these simulation results discussed above, it could be concluded that the air filled in the cavities of ZIF-8 played a significant role in hindering the heat transfer, which may be an important reason for the outstanding thermal stability of CALB-ZIF-8 under extremely high-temperature conditions, where the temperature within the cavities of ZIF-8 would be lower than the outside, thus protecting the enzyme activity under high-temperature conditions.

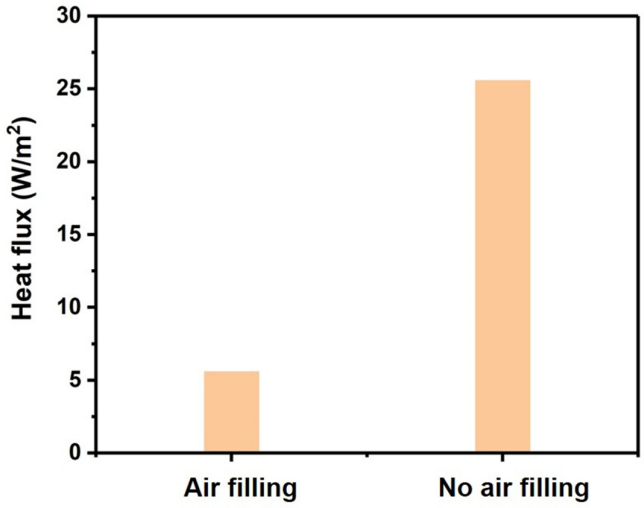

Figure 7. Heat flux of two situations after reaching the steady state.

4. Conclusions

In conclusion, we took CALB-ZIF-8 as an example to synthesize the enzyme-MOF composites via a one-pot precipitation method in an aqueous solution. The as-synthesized CALB-ZIF-8 composites exhibited a uniform size distribution with an average size of 100 nm and outstanding thermal stability, where CALB-ZIF-8 in dry conditions would well maintain their activity at nearly 80% after heating at 180 °C for 10 min which was because the rigidity structure of ZIF-8 may be helpful for the maintenance of the secondary structure of proteins under high temperature. To further study this phenomenon, the finite element method was applied to investigate the heat transfer process within ZIF-8, indicating that the air filled in the cavities of ZIF-8 played a significant role in hindering the heat transfer, which was considered an important reason for the outstanding thermal stability of CALB-ZIF-8 in dry conditions. This study further proved that the immobilization of enzymes in ZIF-8 was an effective way to enhance their stability for long-term catalysis, no matter in aqueous solution or in a solid state, which was of great promise in expanding the application scenario of enzyme-MOF composites.

Supplementary Materials: The following supporting information can be downloaded at: https://www.mdpi.com/article/10.3390/chemistry5030137/s1, Figure S1: EDS mapping of elemental distribution of Zn and S within CALB-ZIF-8; Figure S2: XRD patterns of CALB-ZIF-8 composites; Figure S3: SEM images of CALB-ZIF-8 after heating for different time; Figure S4: XRD patterns of CALB-ZIF-8 after heating for different times; Figure S5: Pictures showing the free CALB and CALB-ZIF-8 before and after heating; Figure S6: TGA data of free CALB and CALB-ZIF-8 when heating at 180 °C for 10 min; Figure S7: CD spectrograms of CALB before and after heating at 180 °C for 10 min.

Author Contributions: Conceptualization and methodology, S.C. and J.G.; experiments and simulation, S.C.; original draft preparation, S.C.; review and editing, J.G. All authors have read and agreed to the published version of the manuscript.

Funding: This research was funded by Shenzhen Science and Technology Innovation Committee, grant number JSGG20220606140403007.

Data Availability Statement: This study did not report any data.

Conflicts of Interest: The authors declare no conflict of interest.

References

1. Sun, H.; Zhang, H.; Ang, E.L.; Zhao, H. Biocatalysis for the synthesis of pharmaceuticals and pharmaceutical intermediates. *Bioorgan. Med. Chem.* **2018**, *26*, 1275–1284. [CrossRef]
2. Choi, J.M.; Han, S.; Kim, H.S. Industrial applications of enzyme biocatalysis: Current status and future aspects. *Biotechnol. Adv.* **2015**, *33*, 1443–1454. [CrossRef]
3. Sun, H.; Li, Y.; Yu, S.; Liu, J. Metal-organic frameworks (MOFs) for biopreservation: From biomacromolecules, living organisms to biological devices. *Nano Today* **2020**, *35*, 100985. [CrossRef]
4. Panganiban, B.; Qiao, B.; Jiang, T.; DelRe, C.; Obadia, M.M.; Nguyen, T.D.; Smith, A.A.A.; Hall, A.; Sit, I.; Crosby, M.G.; et al. Random heteropolymers preserve protein function in foreign environments. *Science* **2018**, *359*, 1239–1243. [CrossRef] [PubMed]
5. Wilner, O.I.; Weizmann, Y.; Gill, R.; Lioubashevski, O.; Freeman, R.; Willner, I. Enzyme cascades activated on topologically programmed DNA scaffolds. *Nat. Nanotechnol.* **2009**, *4*, 249–254. [CrossRef]
6. Ge, J.; Lei, J.; Zare, R.N. Protein-inorganic hybrid nanoflowers. *Nat. Nanotechnol.* **2012**, *7*, 428–432. [CrossRef] [PubMed]
7. Liang, W.; Wied, P.; Carraro, F.; Sumby, C.J.; Nidetzky, B.; Tsung, C.K.; Falcaro, P.; Doonan, C.J. Metal-organic framework-based enzyme biocomposites. *Chem. Rev.* **2021**, *121*, 1077–1129. [CrossRef] [PubMed]
8. Cao, Y.; Ge, J. Hybrid enzyme catalysts synthesized by a de novo approach for expanding biocatalysis. *Chin. J. Catal.* **2021**, *42*, 1625–1633. [CrossRef]
9. Cai, G.; Yan, P.; Zhang, L.; Zhou, H.; Jiang, H. Metal-organic framework-based hierarchically porous materials: Synthesis and applications. *Chem. Rev.* **2021**, *121*, 12278–12326. [CrossRef]
10. Freund, R.; Zaremba, O.; Dinca, M.; Arnauts, G.; Ameloot, R.; Skorupskii, G.; Bavykina, A.; Gascon, J.; Ejsmont, A.; Goscianska, J.; et al. The current status of MOF and COF applications. *Angew. Chem. Int. Edit.* **2021**, *60*, 23975–24001. [CrossRef]
11. Maurin, G.; Serre, C.; Cooper, A.; Fereyd, G. The new age of MOFs and of their porous-related solids. *Chem. Soc. Rev.* **2017**, *46*, 3104–3107. [CrossRef] [PubMed]
12. Lyu, F.; Zhang, Y.; Zare, R.N.; Ge, J.; Liu, Z. One-pot synthesis of protein-embedded metal-organic frameworks with enhanced biological activities. *Nano Lett.* **2014**, *14*, 5761–5765. [CrossRef]
13. Liang, K.; Coghlan, C.J.; Bell, S.G.; Doonan, C.; Falcaro, P. Enzyme encapsulation in zeolitic imidazolate frameworks: A comparison between controlled co-precipitation and biomimetic mineralisation. *Chem. Commun.* **2016**, *52*, 473–476. [CrossRef]
14. Liang, K.; Ricco, R.; Doherty, C.M.; Styles, M.J.; Bell, S.; Kirby, N.; Mudie, S.; Haylock, D.; Hill, A.J.; Doonan, C.J.; et al. Biomimetic mineralization of metal-organic frameworks as protective coatings for biomacromolecules. *Nat. Commun.* **2015**, *6*, 7240. [CrossRef] [PubMed]
15. Wu, X.; Yue, H.; Zhang, Y.; Gao, X.; Li, X.; Wang, L.; Cao, Y.; Hou, M.; An, H.; Zhang, L.; et al. Packaging and delivering enzymes by amorphous metal-organic frameworks. *Nat. Commun.* **2019**, *10*, 5165. [CrossRef] [PubMed]
16. Chen, G.; Huang, S.; Kou, X.; Zhu, F.; Ouyang, G. Embedding functional biomacromolecules within peptide-directed metal-organic framework (MOF) nanoarchitectures enables activity enhancement. *Angew. Chem. Int. Edit.* **2020**, *59*, 13947–13954. [CrossRef]
17. Chen, G.; Kou, X.; Huang, S.; Tong, L.; Shen, Y.; Zhu, W.; Zhu, F.; Ouyang, G. Modulating the biofunctionality of metal-organic framework-encapsulated enzymes through controllable embedding patterns. *Angew. Chem. Int. Edit.* **2020**, *59*, 2867–2874. [CrossRef]
18. Carraro, F.; Williams, J.D.; Linares-Moreau, M.; Parise, C.; Liang, W.; Amenitsch, H.; Doonan, C.; Kappe, C.O.; Falcaro, P. Continuous-flow synthesis of ZIF-8 biocomposites with tunable particle size. *Angew. Chem. Int. Edit.* **2020**, *59*, 8123–8127. [CrossRef]
19. Hu, C.; Bai, Y.; Hou, M.; Wang, Y.; Wang, L.; Cao, X.; Chan, C.; Sun, H.; Li, W.; Ge, J.; et al. Defect-induced activity enhancement of enzyme-encapsulated metal-organic frameworks revealed in microfluidic gradient mixing synthesis. *Sci. Adv.* **2020**, *6*, eaax5785. [CrossRef]
20. Wu, X.; Xiong, J.; Liu, S.; Zong, M.; Lou, W. A versatile competitive coordination strategy for tailoring bioactive zeolitic imidazolate framework composites. *Small* **2021**, *17*, 2007586. [CrossRef]
21. Garcia-Garcia, P.; Muller, M.; Corma, A. MOF catalysis in relation to their homogeneous counterparts and conventional solid catalysts. *Chem. Sci.* **2014**, *5*, 2979–3007. [CrossRef]
22. Delre, C.; Chang, B.; Jayapurna, I.; Hall, A.; Wang, A.; Zolkin, K.; Xu, T. Synergistic enzyme mixtures to realize near-complete depolymerization in biodegradable polymer/additive blends. *Adv. Mater.* **2021**, *33*, 2105707. [CrossRef]
23. Delre, C.; Jiang, Y.; Kang, P.; Kwon, J.; Hall, A.; Jayapurna, I.; Ruan, Z.; Ma, L.; Zolkin, K.; Li, T.; et al. Near-complete depolymerization of polyesters with nano-dispersed enzymes. *Nature* **2021**, *592*, 558–563. [CrossRef] [PubMed]
24. Huang, Q.; Hiyama, M.; Kabe, T.; Kimura, S.; Iwata, T. Enzymatic self-biodegradation of poly(L-lactic acid) films by embedded heat-treated and immobilized Proteinase K. *Biomacromolecules* **2020**, *21*, 3301–3307. [CrossRef] [PubMed]
25. Liu, Y.; Cao, X.; Ge, J. Antioxidative composites based on multienzyme systems encapsulated in metal-organic frameworks. *ACS Appl. Mater. Inter.* **2021**, *13*, 46431–46439. [CrossRef]
26. Velasquez-Hernandez, M.D.; Ricco, R.; Carraro, F.; Limpoco, F.T.; Linares-Moreau, M.; Leitner, E.; Wiltsche, H.; Rattenberger, J.; Schrottner, H.; Fruhwirt, P.; et al. Degradation of ZIF-8 in phosphate buffered saline media. *Crystengcomm* **2019**, *21*, 4538–4544. [CrossRef]

27. Zhou, K.; Mousavi, B.; Luo, Z.X.; Phatanasri, S.; Chaemchuen, S.; Verpoort, F. Characterization and properties of Zn/Co zeolitic imidazolate frameworks vs. ZIF-8 and ZIF-67. *J. Mater. Chem. A* **2017**, *5*, 952–957. [CrossRef]
28. Pan, Y.; Liu, Y.; Zeng, G.; Zhao, L.; Lai, Z. Rapid synthesis of zeolitic imidazolate framework-8 (ZIF-8) nanocrystals in an aqueous system. *Chem. Commun.* **2011**, *47*, 2071–2073. [CrossRef]
29. Shieh, F.K.; Wang, S.; Yen, C.; Wu, C.; Dutta, S.; Chou, L.; Morabito, J.V.; Hu, P.; Hsu, M.H.; Wu, K.C.W.; et al. Imparting functionality to biocatalysts via embedding enzymes into nanoporous materials by a de novo approach: Size-selective sheltering of catalase in metal-organic framework microcrystals. *J. Am. Chem. Soc.* **2015**, *137*, 4276–4279. [CrossRef]
30. Maddigan, N.K.; Linder-Patton, O.M.; Falcaro, P.; Sumby, C.J.; Bell, S.G.; Doonan, C.J. Influence of the synthesis and storage conditions on the activity of candida antarctica lipase B ZIF-8 biocomposites. *ACS Appl. Mater. Inter.* **2021**, *13*, 51867–51875. [CrossRef]
31. Butonova, S.A.; Ikonnikova, E.V.; Sharsheeva, A.; Chernyshov, I.Y.; Kuchur, O.A.; Mukhin, I.S.; Hey-Hawkins, E.; Vinogradov, A.V.; Morozov, M.I. Degradation kinetic study of ZIF-8 microcrystals with and without the presence of lactic acid. *RSC Adv.* **2021**, *11*, 39169–39176. [CrossRef] [PubMed]
32. Liang, W.; Cheng, J.; Zhang, J.; Xiong, Q.; Jin, M.; Zhao, J. pH-Responsive on-demand alkaloids release from core-shell ZnO@ZIF-8 nanosphere for synergistic control of bacterial wilt disease. *ACS Nano* **2022**, *16*, 2762–2773. [CrossRef] [PubMed]
33. Lee, M.J.; Kwon, H.T.; Jeong, H.K. High-flux zeolitic imidazolate framework membranes for propylene/propane separation by postsynthetic linker exchange. *Angew. Chem. Int. Edit.* **2018**, *57*, 156–161. [CrossRef] [PubMed]
34. Ying, P.; Zhang, J.; Zhang, X.; Zhong, Z. Impacts of functional group substitution and pressure on the thermal conductivity of ZIF-8. *J. Phys. Chem. C* **2020**, *124*, 6274–6283. [CrossRef]
35. Zhang, X.; Jiang, J. Thermal conductivity of zeolitic imidazolate framework-8: A molecular simulation study. *J. Phys. Chem. C* **2013**, *117*, 18441–18447. [CrossRef]